Journal of Solid State Chemistry 183 (2010) 2770–2778

Contents lists available at ScienceDirect

Journal of Solid State Chemistry

journal homepage: www.elsevier.com/locate/jssc

Crystal structure, thermal and magnetic properties of $Cr_2V_4O_{13}$

S.J. Patwe [a], S.N. Achary [a,*], J. Manjanna [a], R.M. Kadam [b], H.G. Salunke [c], A.K. Tyagi [a]

[a] Chemistry Division, Bhabha Atomic Research Centre, Mumbai 40085, India
[b] Radio Chemistry Division, Bhabha Atomic Research Centre, Mumbai 40085, India
[c] Technical Physics Division, Bhabha Atomic Research Centre, Mumbai 40085, India

ARTICLE INFO

Article history:
Received 30 March 2010
Received in revised form
2 September 2010
Accepted 12 September 2010
Available online 21 September 2010

Keywords:
Vanadate
Crystal structure
X-ray diffraction
Rietveld refinement
Electron paramagnetic resonance
Magnetic properties

ABSTRACT

$Cr_2V_4O_{13}$, a tetravanadate of Cr^{3+} has been prepared by repeated heating of stoichiometric amounts of Cr_2O_3 and V_2O_5 and its crystal structure is refined by Rietveld refinement of the powder XRD data. This compound crystallizes in a monoclinic lattice with unit cell parameters: $a=8.2651(3)$, $b=9.2997(3)$, $c=14.5215(5)$ Å, $\beta=102.618(3)^\circ$, $V=1089.21(6)$ Å^3 and $Z=4$ (Space group: $P2_1/c$). The U shaped $(V_4O_{13})^{6-}$ formed by corner connected VO_4 tetrahedra links the Cr_2O_{10} (dimers of two edge shared CrO_6 octahedra) forming a three dimensional network structure of $Cr_2V_4O_{13}$. This compound is stable up to 635 °C and peritectically decomposes to orthorhombic $CrVO_4$ and V_2O_5 above this temperature. A possible long range antiferromagnetic ordering below 10 K is suggested from the squid magnetometry and electron paramagnetic resonance (*epr*) spectroscopic studies of $Cr_2V_4O_{13}$.

1. Introduction

Complex vanadates are of interest in basic and applied research due to their diversified crystal chemistry resulting from the linkages vanadium oxygen polyhedra as well as effective catalytic, electrochemical and ion conducting properties [1–6]. Crystal structures of most of the vanadates are built from the VO_4 or VO_5 polyhedra. The linkages of these polyhedra depend on the nature of the counter cations and stoichiometry which in turn decide the crystal structure of the vanadates. The tetrahedral vanadium oxygen polyhedra have been observed as isolated units in orthovanadates and as infinite chains of corner-linked VO_4 units in metavanadates. Besides, clusters of VO_4 tetrahedral units as $(V_nO_{3n+1})^{(n+2)-}$ with $n=2$, 3 ,4, etc., are also observed in several vanadates [1–3]. The complex vanadates of transition metal ions have a wide range of catalytic applications [7]. Efficient and selective catalytic activities for several chemical reactions have been reported for complex vanadates of chromium [8,9]. In particular, compounds in vanadium rich region of V_2O_5–Cr_2O_3 system or Cr^{3+} substituted vanadium oxides are more promising for such applications [10,11].

In the search of new Cr^{3+} containing vanadium oxides, phase relations in V_2O_5–Cr_2O_3 system have been studied in several reports [11–20]. The most common observation of these studies is the existence of $CrVO_4$. However, Olivier [16] have mentioned about the existence of $Cr_2V_4O_{13}$, a vanadium rich phase in V_2O_5–Cr_2O_3 system. Several reports in literature also support the existence of $Cr_2V_4O_{13}$ phase in the low temperature reactions of V_2O_5 and Cr_2O_3 [16–18]. In these reports, the authors have suggested $Cr_2V_4O_{13}$ is a metastable compound with a frame of Cr–O–$Cr(VO_4)_3$ and decomposes to $CrVO_4$ and V_2O_5 above 566 °C. The existence of this phase is confirmed from the thermal analysis and X-ray diffraction studies by Walczak and Filipek [19]. Touboul and Melghit have prepared different polymorphs of $CrVO_4$ and $Cr_2V_4O_{13}$ by careful dehydration of amorphous hydrated forms of vanadates of chromium [21]. Filipek et al. [20] prepared $Cr_2V_4O_{13}$ by different preparation techniques and characterized by powder XRD and Infrared spectroscopy. From the powder XRD data a monoclinic lattice has been assigned to this composition [20]. Analogous composition in V_2O_5–Fe_2O_3 system could be successfully prepared and crystal structure was elucidated from the powder XRD data [22]. Wang et al. [23] have reported crystal structure of $Fe_2V_4O_{13}$ and its Mo substituted derivative from single crystal XRD studies. However, the authors have mentioned that these compositions exist as minor phases in the annealed products of component oxides [23]. The crystal structure analysis of $Fe_2V_4O_{13}$ revealed the presence of a cyclo vanadates with unique architect of U shape and Fe_2O_{10} (octahedral dimer). Such cyclic arrangements of four tetrahedra have been earlier reported for an identical composition $Cr_2P_4O_{13}$ in Cr_2O_3–P_2O_5 system [24]. A comparison of $Cr_2P_4O_{13}$ and $Fe_2V_4O_{13}$ shows a close similarity in crystal structure. Recently, Pozdnyakova et al. [25] have given a structure model for $Cr_2V_4O_{13}$ from powder XRD data. The structural parameters proposed by Pozdnyakova et al. [25]

* Corresponding author. Fax: +91 22 25505151.
E-mail addresses: sachary@barc.gov.in, sachary@apsara.barc.ernet.in (S.N. Achary), aktyagi@barc.gov.in (A.K. Tyagi).

0022-4596/$ - see front matter © 2010 Elsevier Inc. All rights reserved.
doi:10.1016/j.jssc.2010.09.015

have similar unit cell parameters as those reported by Filipek et al. [20]. However, the position coordinates and numbers of atoms in the unit cell show drastic abnormalities in inter-atomic distances. In addition the observed powder XRD pattern of Pozdnyakova et al. [25] appears quite different from that reported by Filipek et al. [20]. A continuous solid solution between $Cr_2V_4O_{13}$ and $Fe_2V_4O_{13}$ [26] suggests both the end members should be isostructural. However, the complicated and irreproducible preparation, kept $Cr_2V_4O_{13}$ as an unexplored crystal structure.

Gron et al. [27,28] have reported magnetic and electrical properties of $Cr_2V_4O_{13}$. Tunable semiconducting properties similar to $Fe_2V_4O_{13}$ are also reported for $Cr_2V_4O_{13}$ [27]. Antiferromagnetic transition with $T_N \sim 13$ K and a metamagnetic transition have been reported for $Cr_2V_4O_{13}$ and its Mo-substituted derivatives [28]. The electron paramagnetic resonance spectroscopic studies on $Cr_2V_4O_{13}$ indicates its antiferromagntic transition with $T_N = 7$ K and g factor 1.97 [27]. Sunandana has observed multiplets in the *epr* spectra for a similar composition and suggested different oxidation state of Cr and V [29]. Due to lack of phase pure crystalline sample and a proper crystal structure, the details of magnetic behavior have not been clarified [28]. In order to elucidate the crystal structure of $Cr_2V_4O_{13}$, phase pure sample was prepared. The thermal stability and magnetic properties of $Cr_2V_4O_{13}$ were also investigated. The details of preparation, crystal structure, thermal stability and magnetic properties of $Cr_2V_4O_{13}$ are presented in this report.

2. Experimental

The title compound was prepared by solid state reaction of stoichiometric amounts of V_2O_5 and Cr_2O_3 at 630 °C. The completion of the reaction was monitored by recording the powder XRD pattern of the sample after each heat treatment. The XRD patterns were recorded on a Philips Powder X-ray diffractometer (model PW1710) using the Cu$K\alpha$ radiation ($K_{\alpha1} = 1.5406$ Å and $K_{\alpha2} = 1.5444$ Å). The dark brownish product obtained after the final heat treatment was used in this study. The thermal stability of the sample was studied by thermogravimetry using Setaram simultaneous TG-DTA set up (model TG-DTA 92-16). The XRD patterns of the samples retrieved after heating at different temperatures were also analyzed.

The diffraction data for structural analysis was collected on a Philips X'pert Pro X-ray diffractometer in reflection mode using the Cu$K\alpha$ ($K_{\alpha1} = 1.5406$ Å and $K_{\alpha2} = 1.5444$ Å) radiation. Well ground sample was smeared on a perspex sample holder. The diffraction data was collected in the 2θ range of 10–120° in step width and time of 0.02° and 4.5 s, respectively. The observed profile of powder XRD pattern was refined by Rietveld method using Fullprof-2K software package [30]. The high temperature XRD patterns of the sample were recorded in the angular range of 10–70° with step width and time of 0.02 and 0.5 s, respectively. Well ground sample was smeared on a platinum strip sample holder cum heater. The sample was heated to a desired temperature and equilibrated for 5 min before collection of data.

The variation of magnetization with temperature of the polycrystalline sample was studied in zero field and field cooled conditions using a Squid magnetometer (quantum design) with an applied field of 100 Oe. The field dependent magnetizations (M vs. H) at several temperatures between 2 and 300 K were also recorded. The *epr* spectra of polycrystalline sample were recorded on a Bruker ESP-300 spectrometer operated at X-band frequency (9.5 GHz), 100 kHz frequency modulation. A phase sensitive detector was used to obtain a first derivative and second derivative signal. Di phenyl picryl hydrazyl (DPPH) was used for calibration of g-values of paramagnetic species. The variable temperature *epr* spectra were recorded in the temperature range of 80–300 K using a variable temperature accessory, viz. Eurotherm B-VT 2000. The *epr* parameters (g parameter, line width and intensity) were precisely determined from the calculated spectra using Bruker SIMFONIA and WINEPR program.

3. Results and discussion

The progress of the reaction of Cr_2O_3 and V_2O_5 was monitored by analyzing the XRD patterns recorded after different heat treatment. The reactant mixture heated at 500 or 550 °C do not show any new reflection except those for the Cr_2O_3 and V_2O_5. However, heating the mixture at 600–650 °C shows the appearance of new reflections similar to those reported by Filipek et al. [20]. Thus an optimum reaction temperature (630 °C) is adopted for the preparation of $Cr_2V_4O_{13}$. In spite of the reaction temperature close to melting temperature of vanadium oxide, the reaction does not complete in a single continuous heating. Almost single phasic sample could be obtained after heating four times at 630 °C (each for 3 h). Each time the sample was slowly cooled to room temperature rehomogenized and pelletized for next heating. In addition, no reflection due to $CrVO_4$ is observed in the final product. This suggests that the reaction does not proceed through the reaction between $CrVO_4$ and V_2O_5, instead through a direct reaction between Cr_2O_3 and V_2O_5.

The powder XRD pattern of $Cr_2V_4O_{13}$ obtained after final heat treatment is shown in Fig. 1. The observed XRD pattern closely agrees with the data reported by Filipek et al. [20] and Touboul and Melghit [21]. The present observed intensity distribution in the XRD pattern appears quite different from that reported for $Cr_2V_4O_{13}$ prepared by low temperature soft chemistry route [25]. It can also be mentioned here that the observed XRD pattern does not show any similarity with the hydrated phases of $Cr_2V_4O_{13}$ prepared by precipitation method [16,17]. The anhydrous nature of the present studied $Cr_2V_4O_{13}$ sample is further confirmed by thermogravimetry, which has been explained later in this paper. The reported reflections for $Cr_2V_4O_{13}$ [20] are marked in Fig. 1 for comparison. In addition, there are several weak reflections unaccounted by this unit cell were assigned to V_2O_5 [32]. A monoclinic lattice with unit cell parameters: $a = 8.2663(17)$, $b = 9.3033(26)$, $c = 7.5373(16)$ Å and $\beta = 109.638(37)°$ is reported

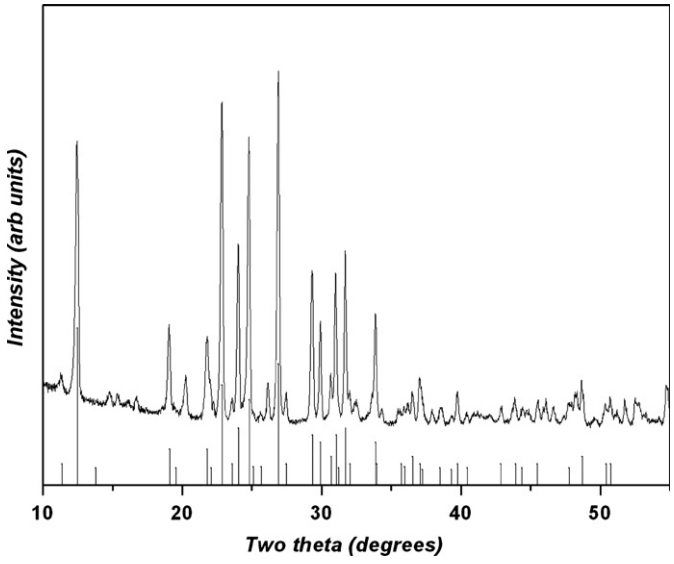

Fig. 1. Observed powder XRD pattern of $Cr_2V_4O_{13}$ (vertical lines corresponds to the data reported by Filipek et al. [20]).

for $Cr_2V_4O_{13}$ [20]. These unit cell parameters are similar to those reported for Mo substituted $Fe_2V_4O_{13}$ [23] and $In_2V_4O_{13}$ [31]. Further analyses of the XRD data were carried out by the Rietveld refinements. Initial trials for the Rietveld refinements were carried out with a model based on the Mo-substituted $Fe_2V_4O_{13}$ (i.e., $Fe_2V_{3.16}Mo_{0.84}O_{13.42}$) with the reported unit cell parameters of Filipek et al. [20]. However, several reflections could not be accounted by this model. It can be mentioned here that crystal structure of $Fe_2V_4O_{13}$ and Mo-substituted $Fe_2V_4O_{13}$ are identical in the aspect octahedral dimer and $(M_4O_{13})^{6-}$ (M=V or V/Mo) units. But the disorder and extra oxygen due to Mo^{6+} ions lead to a subcell for $Fe_2V_{3.16}Mo_{0.84}O_{13.42}$ and all equivalent Fe_2O_{10} dimer instead of two distinct type dimers of $Fe_2V_4O_{13}$. The presently observed two non-equivalent Cr^{3+} ions (also supported by *epr*) supports the doubled unit cell suggested by Filipek et al. [20]. All the observed reflections in the powder XRD data could be indexed on a monoclinic lattice with unit cell parameters: a=8.253(7), b=9.295(5), c=15.03(10) Å, β=102.68(5)°. These unit cell parameters are quite similar to those reported for $Fe_2V_4O_{13}$ [23] and $Cr_2P_4O_{13}$ [24]. In addition these unit cell parameters can be compared to the values reported by Filipek et al. [20], Touboul and Melghit [21] for $Cr_2V_4O_{13}$ and Touboul et al. [31] for $In_2V_4O_{13}$ by doubling one of (c-axis) the unit cell parameters.

The Rietveld refinement of the powder XRD data was carried out using an initial structural model based on $Fe_2V_4O_{13}$ [23] with the above mentioned unit cell parameters. The background of the powder XRD data was modeled by linear interpolation of automatic selected background points using Winplotr interface of Fullprof-2000 software package. Initially the scale and unit cell parameters were refined. The diffractometer zero was fixed at the value observed for standard silicon data. The profile of both $Cr_2V_4O_{13}$ and V_2O_5 phases were fitted using Pseudo-Voigt profile functions. The refined unit cell parameters of $Cr_2V_4O_{13}$ are: a=8.2651(3), b=9.2997(3), c=14.5215(5) Å, β=102.618(3)° and V=1089.21(6) Å^3. After a better profile match, the position coordinates were refined with only one overall thermal parameter. Later on the overall thermal parameters were assigned to individual atoms. Then the position coordinates of all atoms together with all the profile parameters were refined. For the second phase V_2O_5 (orthorhombic, *Pnma*) only scale, unit cell parameters and profile parameters were refined. The quantitative estimation indicates that V_2O_5 phase is about 2 wt%. Finally, the individual thermal parameters of each atom were refined along with the scale, keeping all other parameters fixed. In final cycle these refined thermal parameters were kept fixed due to severe correlation effects. The final refined crystallographic data and profile parameters are given in Table 1. The refined position coordinates of various atoms are given in Table 2. The observed and calculated diffraction patterns along with the difference plot are shown in Fig. 2.

The analyses of the refined structural parameters confirmed isostructural nature of $Cr_2V_4O_{13}$ and $Fe_2V_4O_{13}$. The unit cell consists of crystallographically distinct two chromium (Cr(1) and Cr(2)) and four vanadium (V(1), V(2), V(3) and V(4)) atoms in the unit cell. There are 13 distinct oxygen (O1–O13) atoms present in the unit cell. All the atoms are occupied in the general (4*c*) positions of the space group $P2_1/c$. The analyses of the derived structural parameters indicate that both the chromium (Cr(1) and Cr(2)) atoms have octahedral coordination with Cr–O bonds ranging between 1.89 and 2.12 Å. All the four vanadium atoms have tetrahedral coordination with oxygen atoms and the typical V–O distances are in between 1.63 and 1.84 Å. Such variation of V–O bond lengths is commonly observed in the network vanadates. The observed inter-atomic distances of various atoms in $Cr_2V_4O_{13}$ are given in Table 3. A typical three dimensional representation of the $Cr_2V_4O_{13}$ is shown in Fig. 3. Four of VO_4 tetrahedra are linked together forming U shaped $(V_4O_{13})^{6-}$ units. Two of CrO_6 octahedral units are linked by sharing one edge to form Cr_2O_{10} octahedral dimer units. The typical Cr–Cr distances are 2.93 and 3.16 Å, which are close to the edge shared octahedral CrO_6 structures. These octahedral dimers are aligned along the a-axis of the unit cell. The $(V_4O_{13})^{6-}$ units connect the Cr_2O_{10} units forming a three directional lattice. The distinct cyclic U shaped $(V_4O_{13})^{6-}$ units and dimers of two octahedra as Cr_2O_{10} or Fe_2O_{10} units are the common features in such polyvanadate structures. A typical link of a $(V_4O_{13})^{6-}$ unit to Cr_2O_{10} units in $Cr_2V_4O_{13}$ structure is shown in Fig. 4. It can be mentioned here that the $Cr(1)O_6$ units are connected to other $Cr(1)O_6$ unit through the O4–O4 common edge forming $Cr(1)_2O_{10}$ dimer. Similarly the $Cr(2)_2O_{10}$ dimers are formed by sharing the common O7–O7 edge of $Cr(2)O_6$ octahedra. The typical Cr(1)–O4–Cr(1)

Table 1
Refined crystallographic and other refinement parameters for $Cr_2V_4O_{13}$.

Molecular formula	$Cr_2V_4O_{13}$
Molecular weight	515.76
Space Group	$P2_1/c$ (no. 14)
a, b, c and β	8.2651(3) Å, 9.2997(3) Å, 14.5215(5) Å, 102.618(3)°
Volume and Z	1089.21(6) Å^3, 4
Density (calculated)	3.145 g/cm^3
Angle range, Step width and time	10–120°, 0.02°, 5 s
Diffractometer	Philips X'pert Pro
Wavelengths (Cu$K\alpha$)	1.5406 and 1.5444 Å
Refinement	Rietveld refinements (Fullprof-2K) [ref]
Number of free parameters	78
Background	Linear interpolation of 70 selected points
Number of reflections	3412/2
Profile	Pseudo-Voigt
(U, V, W) η and X	0.55(1), −0.40(1), 0.0916(2), 0.49(2), 0.0022(9)
Pref. orient. parameters	−0.002 (001 directions)
Asym. Parameters: A1 and A2	0.061(3), 0.029(1)
Zero-point	−0.0543 (fixed)
Goodness-of-fit (χ^2)	2.87
$dw_{stat.}$	0.76
R_p, R_{wp} and R_{exp}	7.24, 9.60,5.67
R_B and R_F	7.02. 4.15

2nd phase: V_2O_5 (space group: *Pmnm*).
11.509(2), 4.375(1), 3.558(1), 179.13(6) (fraction: 2 wt%).

Table 2
Refined position coordinates of various atoms in $Cr_2V_4O_{13}$ structure.

Atoms	Site	x	y	z	B_{iso} (Å)^2
Cr1	4*c*	0.1804(4)	0.5050(4)	0.0126(2)	1.666
Cr2	4*c*	0.3058(4)	−0.0052(3)	0.9890(2)	1.257
V1	4*c*	0.5370(8)	0.2049(7)	0.5980(4)	1.212
V2	4*c*	7404(72)	0.2236(7)	0.8214(5)	2.554
V3	4*c*	0.1600(8)	0.2449(6)	0.8279(4)	1.463
V4	4*c*	0.9676(7)	0.7919(7)	0.9064(4)	0.898
O1	4*c*	0.374(2)	0.621(2)	0.982(2)	3.729
O2	4*c*	0.306(2)	0.622(2)	0.132(1)	2.707
O3	4*c*	0.360(2)	0.382(2)	0.087(1)	1.509
O4	4*c*	0.002(1)	0.390(1)	0.057(1)	1.509
O5	4*c*	0.184(3)	0.393(2)	0.890(1)	1.619
O6	4*c*	0.302(2)	0.113(2)	0.865(1)	1.509
O7	4*c*	0.510(1)	0.123(1)	0.044(2)	1.900
O8	4*c*	0.353(2)	0.868(2)	0.106(1)	3.081
O9	4*c*	0.154(2)	0.856(2)	0.922(1)	1.509
O10	4*c*	0.153(2)	0.294(3)	0.711(1)	3.060
O11	4*c*	0.949(1)	0.174(2)	0.808(1)	1.977
O12	4*c*	0.604(2)	0.218(3)	0.720(1)	3.214
O13	4*c*	0.822(2)	0.870(2)	0.951(1)	1.420

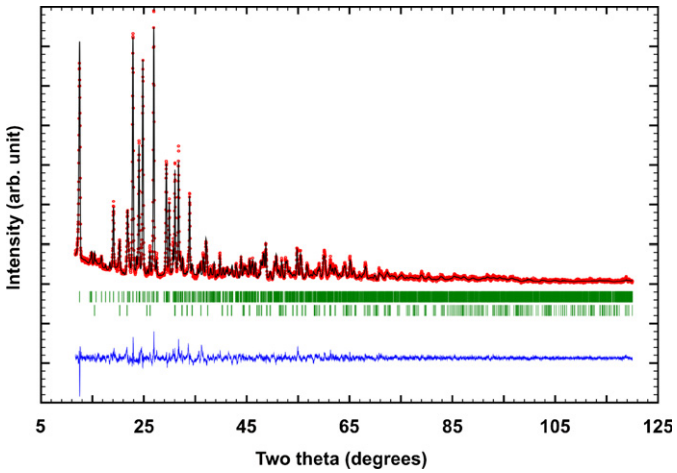

Fig. 2. Observed (circles) and calculated (continuous lines) X-ray diffraction patterns for $Cr_2V_4O_{13}$. The difference plot is shown below the pattern. The vertical bars represent the Bragg positions for $Cr_2V_4O_{13}$ (upper row) and V_2O_5 (lower row).

Table 3
Typical inter-atomic distances (Å) of various atoms and coordination number (CN) of various atoms in $Cr_2V_4O_{13}$.

Cr(1)–O(1)	2.06(2)	Cr(2)–O(6)	2.11(1)
Cr(1)–O2	2.12(2)	Cr(2)–O7	2.08(2)
		Cr(2)–O7	2.02(1)
Cr(1)–O3	2.00(2)	Cr(2)–O8	2.03(2)
Cr(1)–O4	1.89(2)	Cr(2)–O9	1.91(2)
Cr(1)–O4	2.04(2)		
Cr(1)–O5	2.07(2)	Cr(2)–O13	1.97(2)
CN	*6*	*CN*	*6*
V(1)–O1	1.69(2)	V(2)–O11	1.84(2)
V(1)–O3	1.64(2)	V(2)–O12	1.67(2)
V(1)–O7	1.78(2)	V(2)–O2	1.66(2)
V(1)–O12	1.74(1)	V(2)–O8	1.78(2)
CN	*4*	*CN*	*4*
V(3)–O5	1.63(2)	V(4)–O4	1.78(1)
V(3)–O6	1.70(2)	V(4)–O9	1.63(2)
V(3)–O10	1.75(1)	V(4)–O10	1.77(1)
V(3)–O11	1.83(1)	V(4)–O13	1.65(2)
CN	*4*	*CN*	*4*
Cr(1)–Cr(1)	2.925(5)		
Cr(2)–Cr(2)	3.157(5)		
Cr(1)–Cr(2)	4.701(5)	Cr(1)–O4–Cr(1)	96.3(5)°
Cr(1)–Cr(2)	4.885(5)	Cr(2)–O7–Cr(2)	101.0(5)°

and Cr(2)–O7–Cr(2) bond angles are 96.3° and 101.0°, respectively. The O4 and O7 oxygen atoms are connected to two of Cr and one vanadium of $V(4)O_4$ and $V(1)O_4$ tetrahedra. Thus, the $(V_4O_{13})^{6-}$ share all the terminal oxygen (except O10, O11 and O12, which are bridging atoms of the chain) atoms with Cr_2O_{10} octahedral dimers. Such arrangements lead to triangular coordination only for O4 and O7 and linear coordination for rest all oxygen atoms. Thus a flexible framework crystal structure is formed in $Cr_2V_4O_{13}$.

The isolated $(V_4O_{13})^{6-}$ type tertavanadate groups have been reported only in $Fe_2V_4O_{13}$ [23] and $Ba_3V_4O_{13}$ [33]. However, similar isolated $(P_4O_{13})^{6-}$ units have been observed in several phosphates, namely, $Cr_2P_4O_{13}$ [24], $Pb_3P_4O_{13}$ [34], $Bi_2P_4O_{13}$ [35], $Fe_2P_4O_{13}$ [36], $(NbO)_2P_4O_{13}$ [37]. The shape of the present observed $(V_4O_{13})^{6-}$ unit is similar to only that in $Fe_2V_4O_{13}$ and $Cr_2P_4O_{13}$. In all other cases the $(V_4O_{13})^{6-}$ unit**s** are almost linear. A folded cyclic vanadate $(VO_3)_n$ chain has earlier been reported in metavanadates of thorium or neptunium [38,39]. The cyclic chains of these two compounds are infinitely long compared to the distinct isolated fragment of four tetrahedra in the present structure. Due to the presence of more number of the octahedral units, these chains fragmented to isolated $(V_4O_{13})^{6-}$ units.

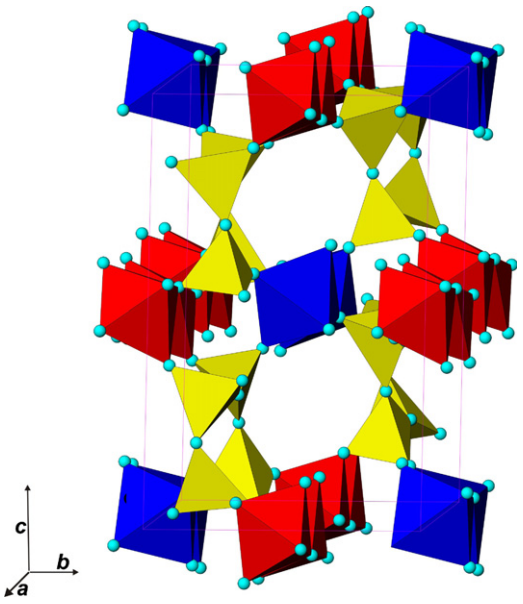

Fig. 3. Crystal structure of $Cr_2V_4O_{13}$ (CrO_6 octahedra and VO_4 tetrahedra are shown).

Another important feature of the framework arrangement of the $(V_4O_{13})^{6-}$ and Cr_2O_{10} units is the formation of a one-dimensional tunnel along the *a*-axis. However, the shape of the tunnel is compressed with shortest O–O separation of about 4 Å and maximum of about 7 Å. It can be mentioned that the selective dehydration of the chromium vanadate may lead to $Cr_2V_4O_{13}$ structure with symmetrical tunnel. Since the structures of hydrated compositions of $Cr_2V_4O_{13}$ are not known, it may not be possible to infer any structural relation between hydrated and dehydrated species.

In order to understand the thermal stability and possible structural transition thermogravimetric (TG), differential thermal analysis (DTA) and *in situ* high temperature XRD studies were carried out. Typical TG-DTA curves for $Cr_2V_4O_{13}$ are shown in Fig. 5. From the thermogravimetric data no weight loss is observed in the temperature range from room temperature to 700 °C. The DTA pattern of $Cr_2V_4O_{13}$ shows a sharp endotherm around 635 °C, which is close to melting point of V_2O_5. From the XRD analysis of the sample the presence of V_2O_5 is concluded to be about 2 wt% only. Thus, this can be either due to melting of V_2O_5 or phase transition at this temperature. The XRD pattern of residue obtained after TG-DTA runs within 700 °C is exactly similar to that of the original compound. The powder XRD patterns of the sample heated at different temperatures are shown in Fig. 6. However, the XRD pattern of the sample obtained after heating $Cr_2V_4O_{13}$ at 800 °C (for 1 h) shows presence of $CrVO_4$ and V_2O_5 (Fig. 6). The stability of $Cr_2V_4O_{13}$ at higher temperature could be clearly observed by *in situ* high temperature XRD studies. The typical XRD patterns recorded at different temperatures are shown in Fig. 7. The characteristic reflections for V_2O_5 (secondary phase, marked in Fig. 6) are persistent up to 600 °C while they totally vanishes in the XRD pattern recorded at 675 °C. In addition the XRD pattern recorded at 675 °C shows new reflections attributable to $CrVO_4$ (marked in Fig. 7). Thus it can be suggested that $Cr_2V_4O_{13}$ continuously decomposes to liquid V_2O_5 and solid $CrVO_4$ above 635 °C. It can also be mentioned here that the rate of decomposition of $Cr_2V_4O_{13}$ is sluggish as observed from the XRD

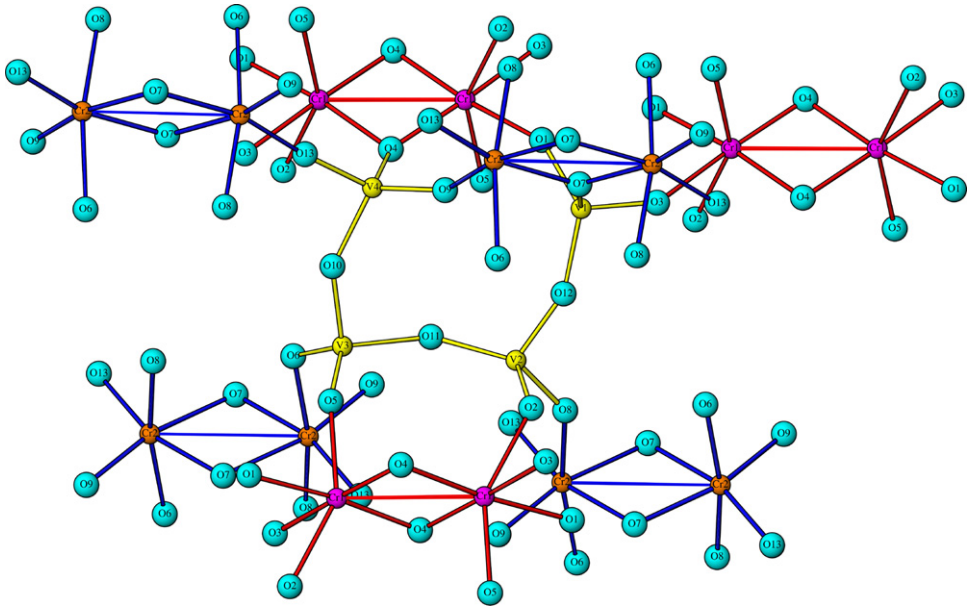

Fig. 4. Typical connection of $(V_4O_{13})^{6-}$ with Cr_2O_{10} dimers.

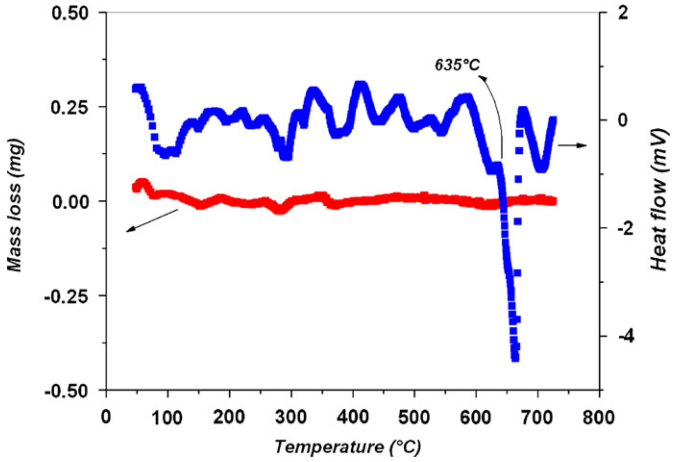

Fig. 5. TG-DTA traces of $Cr_2V_4O_{13}$ (TG-DTA recorded in platinum crucible in static air, heating rate of 10 °C/min).

pattern of the sample recorded after cooling the sample from 675 and 700 °C (for 1 h) The unit cell parameters of $Cr_2V_4O_{13}$ at different temperatures were obtained by Lebail refinement of the corresponding XRD pattern. The refined unit cell parameters at different temperatures are summarized in Table 4. The average coefficient of volume thermal expansion in the temperature range of 25–600 °C is about 16.4×10^{-6}/°C. The lower coefficient of volume thermal expansion can be attributed to relatively open structure of $Cr_2V_4O_{13}$.

The presence of the octahedral dimers with shortest Cr–Cr separation of 2.93 and 3.16 Å, may lead to strong interaction of the spins of Cr^{3+} ions and hence interesting magnetic properties. The temperature dependent magnetization of the sample recorded in field cooled (FC) and zero field cooled (ZFC) conditions are shown in Fig. 8. The ZFC magnetization is lower than the FC magnetization implying an anti-parallel coupling of magnetic moments of Cr atoms. Even for the field as low as 100 Oe, the field cooled magnetization deviates significantly from the ZFC magnetization. The ZFC magnetization does not show any tendency to saturate until 2 K. In this composition, the Cr^{3+} is the only

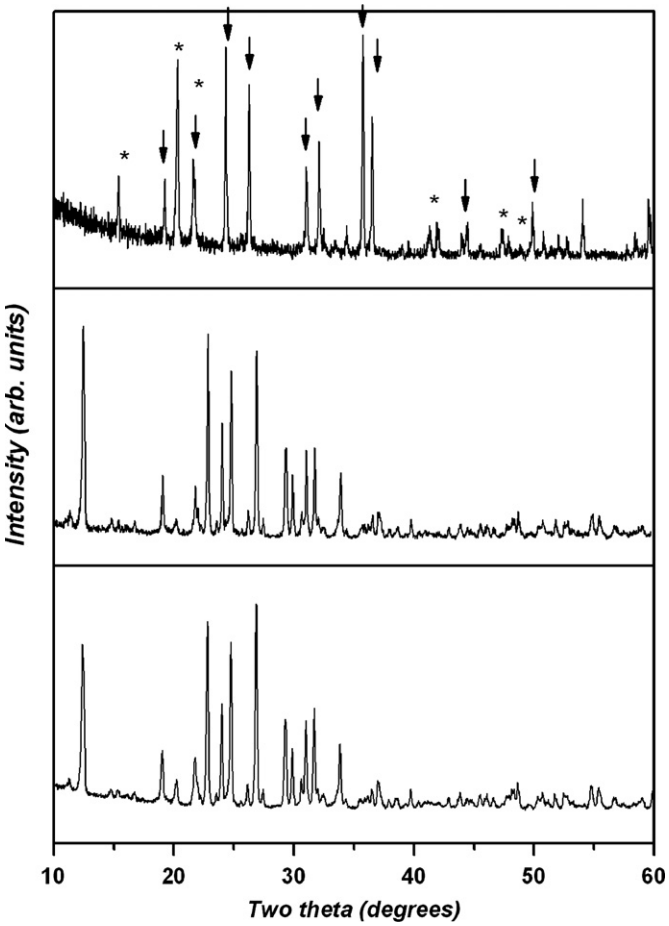

Fig. 6. Powder XRD pattern of (a) as synthesized $Cr_2V_4O_{13}$, (b) after heating up to 700 °C, and (c) and after heating at 800 °C (arrow for $CrVO_4$ and * for V_2O_5) (c).

magnetic ion contributing to the observed magnetization behavior. The absence of lower valence vanadium has been confirmed from the *epr* studies. A broad maximum around 10 K is observed in the variation of magnetization with temperature (*M* vs. *T*).

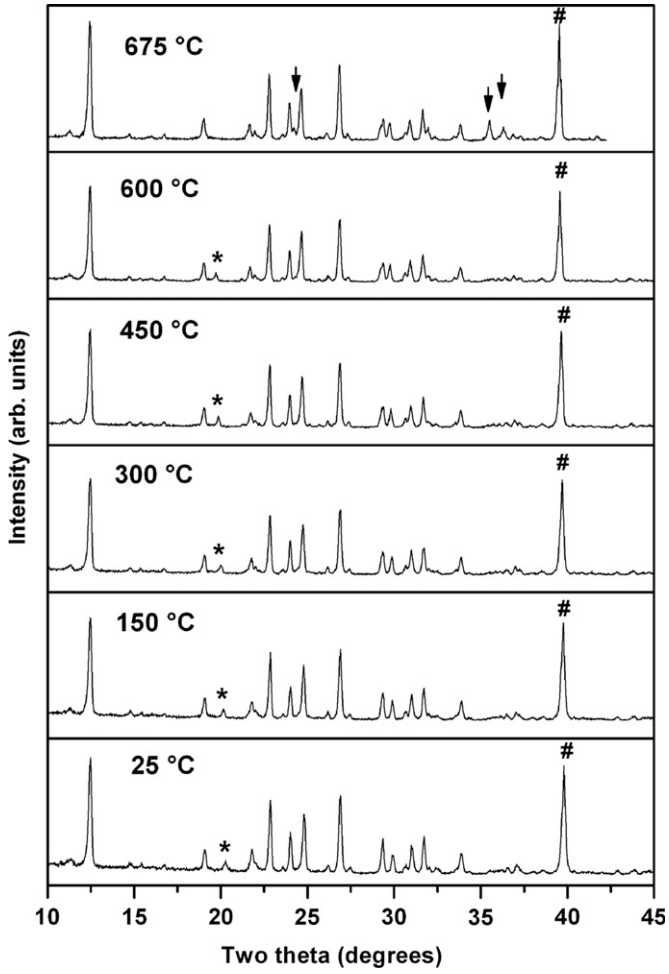

Fig. 7. Powder XRD pattern of $Cr_2V_4O_{13}$ at different temperatures (↓, *, # indicates reflections due to $CrVO_4$, V_2O_5 and Platinum heater).

Table 4
Refined unit cell parameters of $Cr_2V_4O_{13}$ at different temperatures.

Temp (°C)	a (Å)	b (Å)	c (Å)	β (deg)	V (Å)^3
25	8.2639(8)	9.2986(12)	14.5291(12)	102.606(8)	1089.5(2)
150	8.2694(8)	9.3031(12)	14.5356(14)	102.673(10)	1091.0(2)
300	8.2757(8)	9.3090(12)	14.5459(16)	102.806(10)	1092.7(2)
450	8.2870(8)	9.3207(14)	14.5560(18)	102.882(10)	1096.0(2)
600	8.3038(8)	9.3290(16)	14.5702(18)	102.987(14)	1099.8(2)
675	8.3032(10)	9.3309(16)	14.5853(20)	103.170(18)	1100.3(2)

Earlier Gron et al. [27,28] have suggested an antiferromagnetic transition in $Cr_2V_4O_{13}$ around this temperature. However, the maximum in M vs. T is not sharp as expected for a true antiferromagnetic material. This can be attributed to the presence of two different types of super exchange interaction (*intra*-, i.e. within Cr_2O_{10} unit and *inter*-, i.e. between Cr_2O_{10} units mediated by a nonmagnetic VO_4 group). The weak super exchange through the vanadate group gives long range antiferromagnetic ordering in the materials. Magnetic properties of several materials containing such octahedral dimer, viz. Cr_2WO_6, Cr_2TeO_6, $Cr_2Te_4O_{11}$, $Fe_{2-x}Cr_xTeO_6$, etc., have been extensively reported in literature [40–43]. It has been suggested that the 90° super exchanges have shorter cation–cation separation and they are mostly antiferromagnetic in nature [40,42]. The magnetic behaviors of such materials are mainly contributed by the interactions

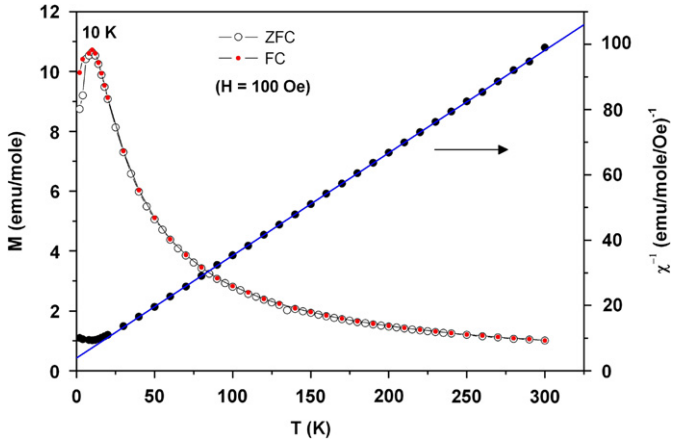

Fig. 8. Variations of magnetization and inverse magnetic susceptibility of $Cr_2V_4O_{13}$ with temperature.

within the octahedral dimers than the inter cluster interactions [40]. However, the weak interactions among the dimers may also play significant role in governing the magnetic order in such compounds. Different possible magnetic interactions between the Cr ions are shown in Fig. 9. The Cr(1)–O4–Cr(1) and Cr(2)–O7–Cr(2) angles in the $Cr_2V_4O_{13}$ are about 96–101°. Thus, the antiferromagnetic interaction between the Cr ions within the dimer is the most favored configuration. From the crystal structure we have observed small but appreciable differences in the Cr(1)–Cr(1) separation and Cr(2)–Cr(2) separations (3.16 and 2.93 Å). Similarly, the Cr(1)–Cr(2) separations also have two different values (4.70 and 4.88 Å). Such variation in the bond length can give rise different short range ordered spin cluster interaction due to differences in the overlap of orbitals. Such differences can produce an inherent magnetic inhomogeneity within the system and hence broadened peak maxima. Thus, the observed cusp at the transition temperature can be attributed to the combined effect of these phenomena.

Fig. 8 also depicts the variation of inverse susceptibility with temperature. A positive intercept in $1/\chi$ vs. T plot indicate an antiferromagnetic interaction. The variation of magnetic susceptibility with temperature could be fitted with Curie–Weiss relation ($\chi = C/T - \vartheta$) with negative Weiss constant ($\vartheta \sim -12.7$ K). The Curie constant estimated from the slope is 4.0(1) (Oe mole K/emu). The Curie constant is given as: $C = N\mu_b^2(p^2)/3kT$, where p is effective moment given by $g\,[(J)(J+1)]^{1/2}$; where N is the number of moles of magnetic atoms. The Curie constant is used to calculate the effective magnetic moment. The effective magnetic moment per Cr^{3+} ion is found to be 3.62 μ_B. The observed moment confirms the d^3 ($S=3/2$) state of Cr atoms. The exchange interaction energy was estimated from the Weiss constant (ϑ) as below

$$\vartheta(\text{in K}) = \frac{2[z_1J_1(S(S+1)+z_2J_2(S(S+1)+z_3J_3(S(S+1)]}{3k}$$

where J_1, J_2 are exchange interaction between the Cr atoms in between the $Cr(1)_2O_{10}$ and $Cr(2)_2O_{10}$ dimers and J_3 represent the interaction energy between the two dimmers. z_1, z_2 and z_3 are 1, 1 and 4, respectively and $S=3/2$.

In the present study, we assumed that the super exchange J_1 and J_2 (Fig. 9) are identical due to small difference in Cr(1)–Cr(1) and Cr(2)–Cr(2) bond lengths. However, the exchange interaction (J_3) between Cr(1)–Cr(2) is relatively weak due to larger separation (Fig. 9) and poor spatial coupling as the exchange integrals are inversely proportional to the distances. In the present case the contribution from J_3 is about half of the J_1 or J_2. Thus, the estimated aggregate interaction energy (J/k) is about

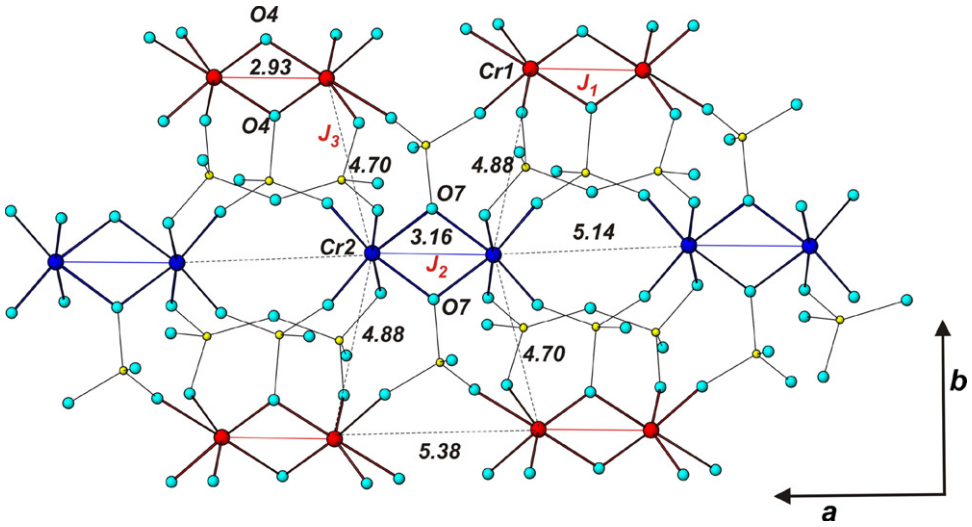

Fig. 9. Typical connections of Cr_2O_{10} dimers and magnetic interactions in $Cr_0V_4O_{13}$ in *ab*-plane (interaction along *c*-direction are not considered due to larger separation).

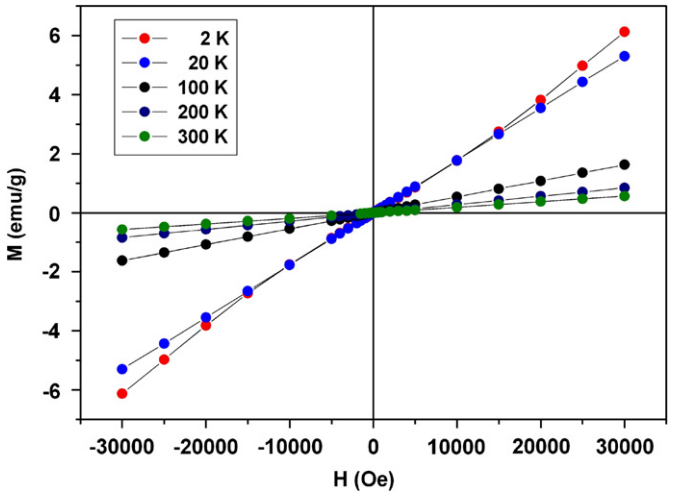

Fig. 10. Variation of magnetization of $Cr_2V_4O_{13}$ with applied field at different temperatures.

−5.0 K. The estimated average exchange energy between the Cr atoms within Cr_2O_{10} is about 3.3 K (0.28 meV). The total magnetic energy at 100 Oe below 10 K is of the order of JP_{eff} (~1.01 meV), which is of the order of thermal energy at 10 K (~1 meV). The lower ordering temperature is due to the lower of exchange coupling and relatively higher magnetic moment of the Cr ions. The variation of molar susceptibility with temperature was further fitted with the relation proposed by Chandramouli et al. [44] for coupled dimers to find the order of J_1 and J_3. The values of J_1 and J_3 are about 1.36 and 0.56 K (Supplementary Information 1).

Hysteresis behaviors of $Cr_2V_4O_{13}$ at different temperatures are shown in Fig. 10. No remanence and coercivity is observed even at lowest temperature which is in agreement with the antiferromagnetic ordering. Since the transition temperature is small the hysteresis replicates a paramagnetic behavior at all temperatures except 2 K. At higher applied field, the hysteresis at 2 K shows upward deviation from the normal paramagnetic like behavior. This deviation may be arising from the breaking Cr–Cr intra dimer coupling at larger field or a spin–flip transition. The detailed magnetic structure determination will be useful to explain the magnetic behavior of $Cr_2V_4O_{13}$. Earlier Gron et al. have indicated a metamagnetic behavior for $Cr_2V_4O_{13}$ and its molybdenum substituted analogues [27,28]. From the observed magnetic moment and negative Weiss constant it can be suggested a possible long range antiferromagnetic ordering in $Cr_2V_4O_{13}$. The long range antiferromagnetic ordering is also supported by *epr* spectroscopic studies.

The electron paramagnetic resonance (*epr*) spectra of polycrystalline sample of $Cr_2V_4O_{13}$ recorded in first and second derivative mode of presentation are shown in Fig. 11. The *epr* spectrum recorded at room temperature in first derivative mode is a single, symmetrical and broad resonance line (shown as inset in Fig. 11). The shape of the resonance signal could be fitted with single Lorentzian line. As the line width become comparable to the resonance field, the contribution of the linearly polarized microwave field dominates the line shape. The registered *epr* line at room temperature is centered at $g=1.9625$, with peak to peak width ≈ 435 G, confirming presence of chromium as Cr^{3+} as concluded from the magnetic measurements. The *epr* spectra recorded in second derivative mode of presentation were more resolved. The *epr* spectrum at 80 K could be easily deconvoluted into two peaks at $g=1.9999$ and 1.9787, respectively. These can be attributed to the presence of Cr^{3+} ions situated in two different types of octahedral coordination differing slightly in bond lengths. This supports to the two different coordination environment of Cr^{3+} ion of the present structural studies compared to single environment as reported for $In_2V_4O_{13}$ type structures.

Earlier, *epr* studies on $Cr_2V_4O_{13}$ by Gron et al. [28] indicate $g=1.97$ which is comparable to that observed in first derivative mode of the present study. However, careful second derivative analysis revealed two components in the *epr* spectra. The epr data reported by Sunandana [29] is quite different from the present observed data as well as that reported by Gron et al. [28]. It may be mentioned here that the bluish black sample studied by Sunadana [29] has been prepared by high temperature equilibrium method. Thus lower valence state of vandium might be origin of multiplet in their *epr* signal. The magnetic interactions in $M_3Fe_4V_6O_{24}$ (M(II)=Zn, Cu, Mn, Mg) have been investigated by *epr* spectroscopy [45–49]. The *epr* signal in the case of $M_3Fe_4V_6O_{24}$ has been attributed to exchange coupled magnetic ions from the analyses of *epr* parameters. The effect of temperature on *epr* parameters (line position, line widths and integrated signal intensity) more pronounced if two different magnetic ions are present in the same sub-lattice. Thus, the *epr* spectra of $Cr_2V_4O_{13}$ were recorded at various temperatures between 80 and 300 K. It is observed that the line position remains almost temperature independent while the line width shows a minimum at about

220 K. This might be due to presence of short range ordered spin cluster interaction producing an inherent magnetic inhomogeneity within the system, which is mentioned earlier in Fig. 9.

The *epr* signal obtained in the first derivative mode was integrated and the area under the curve was estimated by using Bruker WINEPR program (area under the *epr* curve represents susceptibility). Fig. 12 shows plot of the temperature dependence of inverse magnetic susceptibility χ^{-1} (measured from *epr* signal). It may be noted here that the variation of inverse magnetic

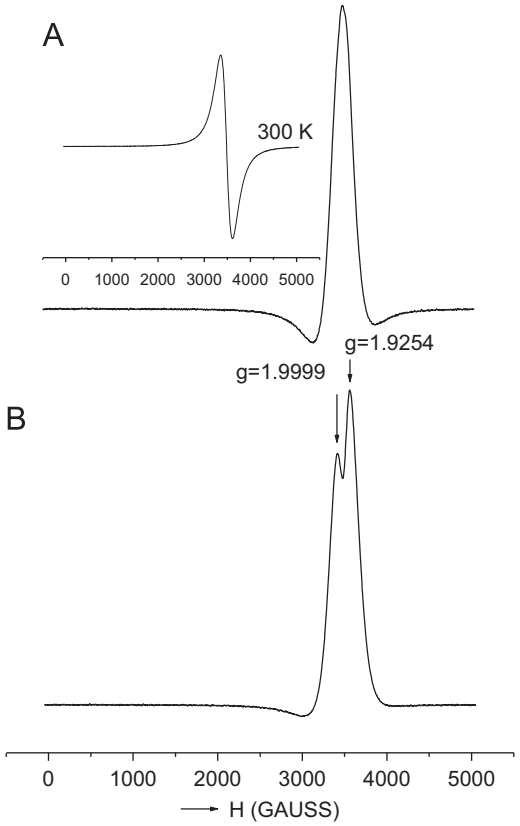

Fig. 11. EPR spectra of $Cr_2V_4O_{13}$ in second derivative presentation (A) 300 K (B) 80 K. (The inset shows *epr* spectra at room temperature in first derivative presentation).

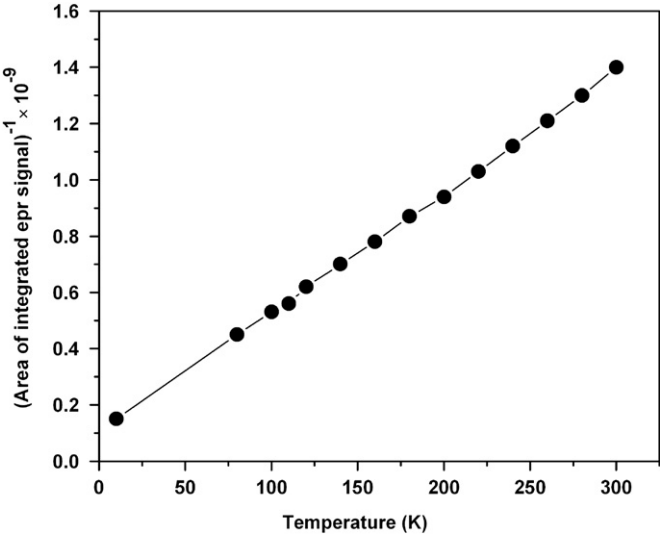

Fig. 12. Variation of the inverse magnetic susceptibility χ^{-1} for $Cr_2V_4O_{13}$ (measured from of *epr* signal) with temperature.

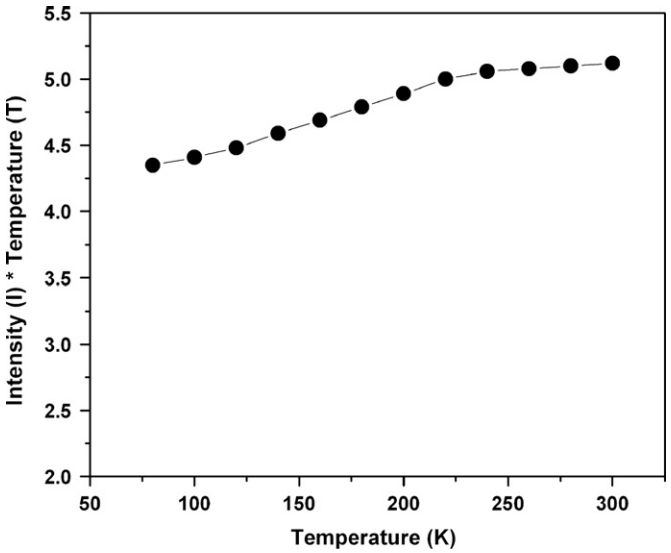

Fig. 13. Temperature dependent variation of the product of integrated intensity and temperature ($I \times T$).

susceptibility with temperature is almost linear and intercepts *Y*-axis as expected for paramagnetic to antiferromagnetic state transition of the system. Further the variation of product of intensity (I) of *epr* signal and temperature (T) with temperature (T) is used to reveal the magnetic behavior of $Cr_2V_4O_{13}$. Typical variation of $I \times T$ with T is shown in Fig. 13. For paramagnetic behavior, $I \times T$ should be independent of T, whereas for ferromagnetic and antiferromagnetic behavior an increase and decrease in $I \times T$ is expected when the temperature is lowered below transition temperature. The decrease of $I \times T$ with decreasing temperature below 220 K (Fig. 13) suggests the paramagnetic to antiferromagnetic transition in $Cr_2V_4O_{13}$.

4. Conclusions

$Cr_2V_4O_{13}$ was successfully synthesized by controlled heat treatment of binary oxides and the crystal structure was refined by Rietveld analysis of the powder XRD data. Preparation and thermal studies revealed a limited stability of this compound. Crystal structure analyses reveal that the lattice is built of Cr_2O_{10} octahedral dimer and U-shaped $(V_4O_{13})^{6-}$ units. The $(V_4O_{13})^{6-}$ units connect the Cr_2O_{10} units by sharing its free corners in all the directions. The framework arrangement of the Cr_2O_{10} and $(V_4O_{13})^{6-}$ units leaves an infinitely long tunnel along *a*-direction. This study also reveals that the observed crystal structure of $Cr_2V_4O_{14}$ is different from that reported by Pozdnyakova et al. [25]. The limited stability of $Cr_2V_4O_{13}$ above 635 °C against the molten V_2O_5 and $CrVO_4$ is concluded from the TG-DTA and *in situ* high temperature XRD studies. The magnetic behavior of $Cr_2V_4O_{13}$ studied by squid magnetometry and *epr* spectroscopy indicates a paramagnetic to long range antiferromagnetic ordering below 10 K.

Acknowledgment

We thank Dr. D. Das [Head, Chemistry Division, Bhabha Atomic Research Centre, Mumbai 400085, India] for supporting this work.

Appendix A. Supplementary Information

Supplementary data associated with this article can be found in the online version at doi:10.1016/j.jssc.2010.09.015.

References

[1] A.F. Wells, in: Structural Inorganic Chemistry, 3rd ed, Oxford University Press, 1962, p. 686.
[2] F.C. Howthorne, C. Calvo, J. Solid State Chem. 22 (1977) 157.
[3] P.Y. Zavalij, M.S. Whittingham, Acta Crystallogr. B55 (1999) 627.
[4] M.S. Whittingham, J. Electrochem. Soc. 123 (1976) 315.
[5] M.S. Whittingham, R. Chen, T. Chirayil, P.Y. Zavalij, Electrochem. Soc. Proc. 96 (1996) 76.
[6] A. Vejux, P. Courtine, J. Solid State Chem. 63 (1986) 179.
[7] H.H. Kung, in: Transition Metal Oxides: Surface Chemistry and Catalysis, Elsevier, Amsterdam, 1989.
[8] C. Pradier, F. Rodrigues, P. Marcus, M. Landau, M. Kaliya, A. Gutman, M. Herskowitz, Appl. Catal. B Environ. 27 (2000) 73.
[9] V. Akifumi, K. Yoshihide, Y. Yasuhisa, S. Yuichi, J. Chem. Soc. Jpn. 9 (1981) 1513.
[10] O. Pozdnyakovaa, E. Kuzmannb, L. Szirtes., Solid State Ionics 161 (2003) 301.
[11] W. Bencsh, E. Worner, M. Muhler, Mater. Res. Bull. 29 (1994) 155.
[12] A. Burdese, Ann. Chim. 47 (1957) 797.
[13] E.C. Completosn, M.Y.C. Simons, B. Barham, Trans. J. Br. Ceram. Soc. 76 (1977) 68.
[14] R.C. Kerby, J.R. Wilson, Can. J. Chem. 51 (1973) 1032.
[15] G. Lucas, M. Weddle, A. Preece, J. Iron Steel Inst. 179 (1955) 342.
[16] D. Olivier, C. R. Acad. Sci. Paris 264C (1967) 1176.
[17] D. Olivier, C. R. Acad. Sci. Paris 272 (1971) 1225.
[18] J. Amiel, D. Olivier, M. Dessolin, C. R. Acad. Sci. Paris 264 (1967) 1045.
[19] J. Walczak, E. Filipek, J. Therm. Anal. 35 (1989) 69.
[20] E. Filipek, J. Walczak, P. Tabero, J. Alloys Compd. 265 (1998) 121.
[21] M. Touboul, K. Melghit, J. Mater. Chem. 5 (1) (1995) 147–150.
[22] L. Permer, Y. Laligant, Eur. J. Solid State Inorg. Chem. 34 (1997) 41.
[23] X. Wang, K.R. Heier, C.L. Stern, K.R. Poeppelmeier, Inorg. Chem. 37 (1998) 6921.
[24] K.H. Lii, Y.B. Chen, C.C. Su, S.L. Wangs, J. Solid State Chem. 82 (1989) 156.
[25] O. Pozdnyakova, J. Megyeri, E. Kuzmann, L. Szirtes, Cent. Eur. J. Chem. 4 (2006) 760.
[26] P. Tabero, E. Filipek, J. Therm. Anal. Calorim. 64 (2001) 1067.
[27] T. Gron, J. Krok, M. Kurzawa, J. Walczak, J. Magn. Magn. Mater. 54 (1986) 1301.
[28] T. Gron, J. Krok-Kowalski, H. Duda, T. Mydlarz, A. Gilewski, J. Walczak, E. Filipek, K. Barner, Phys. Rev. 51 (1995) 16021.
[29] C.S. Sunandana, Mater. Res. Bull. 20 (1985) 531.
[30] J. Rodriguez-Carvajal, Fullprof 2000: a program for Rietveld, profile matching and integrated intensity refinements for X-ray and neutron data, Version 1.6, Laboratoire Leon Brillouin, Gif sur Yvette, France, , 2000.
[31] M. Touboul, K. Melghit, P. Benard, Eur. J. Solid State Inorg. Chem. 31 (1994) 151.
[32] H.G. Bachmann, F.R. Ahmed, W.H. Barnes, Z. Kristallogr. 115 (1961) 110.
[33] B.M. Gatehouse, L.W. Guddat, R.S. Roth, J. Solid State Chem. 71 (1987) 390.
[34] M.T. Averbuch-Pouchot, A. Durif, Acta Crystallogr. C 43 (1987) 631.
[35] M. Bagieu-Beucher, M.T. Averbuch-Pouchot, Z. Kristallogr. 180 (1987) 165.
[36] A.G. Nord, T. Ericsson, P.E. Werner, Z. Krisallogr. 192 (1990) 83.
[37] V.P. Nikolaev, G.G. Sadikov, A.V. Lavrov, M.A. Porai-Koshits, Izv. Akad. Nauk SSSR Neorg. Mater. 22 (1986) 1364.
[38] S.N. Achary, M.R. Pai, R. Mishra, A.K. Tyagi, J. Alloys Compd. 453 (2008) 332.
[39] A. Tabuteau, A. Cousson, M. Pages, M. Gasperin, Acta Crystallogr. B35 (1979) 2000.
[40] M. Drillon, L. Padel, J.C. Bernier, J. Chem. Soc. Faraday II 76 (1980) 1224.
[41] O. Kahn, B. Briat, J. Galy, J. Chem. Soc. Faraday II 73 (1977) 1453.
[42] K. Motida, S. Miyahara, J. Phys. Soc. Jpn. 28 (1970) 1188.
[43] K.D. Singh Mudher, K. Krishnan, I.K. Gopalkrishn, D.C. Kundaliya, S.K. Malik, J. Alloys Compd. 392 (2005) 40.
[44] G.V.R. Chandramouli, C. Balagopalkrishna, M.V. Rajasekharan, P.T. Monoharan, Comput. Chem. 20 (1996) 353.
[45] A. Worsztynowicz, S.M. Kaczmarek, V. Mody, R.S. Czernuszewicz, Rev. Adv. Mater. Sci. 14 (2007) 33.
[46] G. Zolnierkiewicz, N. Guskos, J. Typek, E.A. Anagnostakis, A. Blonska-Tabero, M. Bosacka, J. Alloys Compd. 471 (2009) 28.
[47] G. Zolnierkiewicz, N. Guskos, J. Typekand, A. Blonska-Tabero, Rev. Adv. Mater. Sci. 14 (2007) 119.
[48] N. Guskos, G. Zolnierkiewicz, J. Typek, M. Bosacka, Rev. Adv. Mater. Sci. 14 (2007) 125.
[49] N. Guskos, J. Typek, A. Beskrovnyi, M. Wabia, M. Kurzawa, E.A. Anagnostakis, G. Gasiorek, J. Alloys Compd. 377 (2004) 47.